Ultrafast Dephasing of Single Nanoparticles Studied by Two-Pulse Second-Order Interferometry

Yish-Hann Liau, Andreas N. Unterreiner,† Qing Chang, and Norbert F. Scherer*

Department of Chemistry, James Franck Institute and Materials Research Science and Engineering Center, University of Chicago, 5735 S. Ellis Avenue, Chicago, Illinois 60637

Received: August 4, 2000

Two-pulse second-order interferometric autocorrelation responses of single Ag nanoparticles are reported. The surface plasmon-enhanced second harmonic generation interferogram for single Ag colloids shows significant broadening with respect to the laser pulse second-order autocorrelation. The interferometric autocorrelation response is described and analyzed with a density matrix formalism that incorporates (phenomenologically) the population and the polarization relaxation of the surface plasmon. The total dephasing time (T_2) of the surface plasmon in single Ag colloids is determined to be 10 fs. The present results are compared to previously reported values obtained from ensemble studies of Ag particles and from the line width of the absorption spectrum. Extension of the present ultrafast measurements, the first performed on single nanoparticles, to single molecules studies is discussed.

I. Introduction

The controlled manipulation of the properties of single and multiple particles and structured films is important for the development of new nanostructured devices with tailored photonic functions.[1] Metallic and semiconductor nanoparticles have unique optical and electronic properties.[2−4] The absorptive, luminescent, and nonlinear optical properties of metallic nanoparticles are particularly sensitive to their size and shape.[5−11] The dominant optical resonance of metal particles is associated with a collective electron oscillation, the surface plasmon (SP).[2] Mie scattering theory has been employed to describe the properties of the SP modes and was further improved by incorporating a size-dependent dielectric function of the particles.[12] Other phenomena arise in more complex or extended systems. The collective optical response of multiparticle assemblies can be tuned by controlling the interparticle separation.[13−16] In terms of transport, it has been shown that the SP mode in rough Ag films propagates like a wave in a highly scattering medium.[17] Recently, the propagating mode and the associated dispersion relation were shown to be strongly but controllably altered by periodic modulation of the interfacial dielectric properties.[18] Furthermore, the direct correlation of mesoscopic topographic features with SP-induced reactivity and nanometer-localized electron dynamics has been achieved in ultrafast scanning tunneling microscopy experiments.[19]

Knowledge of the dynamics of electron relaxation is essential for elucidating the unique properties of the metallic states of materials.[20] Upon external electromagnetic perturbation, the conduction electrons in metals are driven to oscillate coherently with the laser field and generate a material polarization. In extended one- and two-dimensional films, the SP mode also carries a net momentum and propagates at the surface of the film. The coherently oscillating electrons eventually lose phase coherence, and the associated polarization diminishes. The electronic dephasing results from pure dephasing processes such as elastic electron−electron collisions and energy-dissipating mechanisms such as radiative decay or relaxation to single-electron eigenstates. These electronic relaxation processes generally take place on femtosecond time scales.[21,22] The dephasing times of SPs in colloidal particles have only been studied in a few cases: by frequency-domain dispersion[23] and by incoherent light degenerate-four-wave-mixing experiments.[24] The subsequent dissipation of electron thermal energy to (nuclear) lattice motion, termed electron−phonon coupling, occurs on hundreds of femtoseconds to picosecond time scales. Thermalization of the lattice occurs on even longer time scales until the whole system reaches equilibrium.

Ultrafast laser systems can now routinely generate 20 fs laser pulses and have been employed to study the electron dynamics of metallic systems.[14,17−19,25−33] The temporal resolution of intensity autocorrelation-based measurements is limited by the width of the autocorrelation function. Because of the extremely short time scale associated with the electronic dephasing, it is often assumed that the electron Fermi sea reaches thermal equilibrium within the (pump) pulse duration. As a result, pump−probe experiments in metallic systems were primarily used to examine electron−phonon coupling or slower processes. By contrast, fringe-resolved interferometric measurements provide a chance to probe ultrafast processes on time scales comparable or shorter than those of the pulse duration by resolving phase shifts or higher harmonic contributions to the measured interferometric response. This technique has been used in studies of the ultrafast dynamics of metallic films,[34,35] structured metal particle arrays,[13,36,37] and bulk semiconductors.[38]

In general, however, most of the experimental investigations in this area have examined ensembles of particles, thereby averaging over a distribution of particle sizes, adding an inhomogeneous contribution to the measured response. Because the electron−phonon dynamics of nanoparticles are strongly affected by their shape (and perhaps size),[8,11,39−41] the dephasing and the relaxation times obtained in these studies should be regarded as a lower limit; the contribution of (structural) inhomogeneity to the dephasing cannot be separated from the

* To whom correspondence should be addressed. E-mail: nfschere@uchicago.edu.

† Present address: Institute of Physical Chemistry, University of Karlsruhe.

10.1021/jp002831x CCC: $20.00
Published on Web 02/23/2001

homogeneous contribution by pump−probe nonlinear spectroscopies. These factors justify the direct investigation of single particles.

To date, only one such investigation has been reported: a frequency domain measurement by near-field scanning optical microscopy. A total dephasing time of about 8 fs was extracted from the line shape of the extinction spectra of single Au particles.[42] However, a range of other measurements has been performed with single metal particles. A study of the STM-induced photon emission from single metal (Au) nanoparticles showed that the localized SP mode of particles is excited by tunneling electrons mainly through an inelastic process.[43] Other investigations utilized the field enhancement associated with SP modes localized on single particles to observe surface-enhanced Raman scattering from single metal particles.[44] Recently, even Raman scattering from (single) molecules adsorbed to single metal nanoparticles has been reported.[45−48]

This paper reports experimental studies of SP dynamics of single Ag colloidal particles. Time-resolved second harmonic generation (SHG) interferometric autocorrelations were measured to obtain the free-induction decay of single particles constituting a more complete report of previously published results.[35] An ensemble of these colloids has an absorption spectrum peaking at around 3.1 eV in solution. Hence, the single-particle interferometric signals are resonantly enhanced because of a two-photon process when exciting with ultrafast laser pulses centered at 800 nm (1.55 eV). The interferometric measurement allows monitoring the phase and amplitude of the optically induced polarization and therefore is a sensitive measure of the coherence relaxation. A density matrix simulation of the interferometric signals is also performed to extract the phase relaxation dynamics of the system. The results are compared to the homogeneous resonance width calculated from Mie theory.

II. Theory and Background

A density matrix formalism has been employed to describe the matter−field interactions.[49] The dynamic properties of the system can be obtained with detailed knowledge of the system−reservoir interaction.[50] However, the essential information is usually incomplete, especially for condensed-phase systems. Nevertheless, the equation of motion that governs the time evolution of the system returning to equilibrium upon external perturbation can be simplified by implementing phenomenological decay rates. The resulting optical Bloch equations employ two characteristic exponential decay rates, $1/T_1$ and $1/T_2$, to describe the population and coherence relaxation of the system, respectively. The optical Bloch equations have been used by others to simulate the coherent field−matter interaction, including the time-resolved photoemission of metallic systems[34,51] and the free-induction decay of semiconductors.[38] In this study, the formalism is adapted to describe the dephasing of the coherently driven plasma oscillation of single Ag nanoparticles.

The laser spectrum, centered at 800 nm, is two-photon resonant with the SP of the Ag colloids; a three-level system is thus used to describe the two-photon-induced process. Upon laser illumination, electrons in the particles are driven coherently by the laser field and undergo collective motion. A nonlinear polarization oscillating at twice the frequency of the laser field, ω, is created. The second harmonic generation from the Ag colloid can be monitored as a function of the delay time to reveal the dynamics of the coherent interaction.

Modeling of the light−matter interaction requires precise characterization of the electric field at the sample. Femtosecond laser systems can generate ultrashort pulses that consist of only a few optical cycles.[52] The electric field of the optical pulse can be reconstructed from the second-order interferometric autocorrelation measured from nonresonant materials with an assumed intensity envelope profile. In the present case, the light field has been characterized at the focus of the microscope objective.[53] The measured SHG interferometric autocorrelation, well approximated as a Gaussian intensity profile, was then used in the simulation described in the following paragraphs.

The system under study is excited by a pair of identical laser pulses that propagate collinearly with a controlled delay. The electric field of the laser pulse pair is

$$E(t) = A(t)\exp[-i\omega t + \phi_1] + A(t+\tau)\exp[-i\omega(t+\tau) + \phi_2] \quad (1)$$

where $A(t)$ is the envelope of the laser field (i.e., Gaussian profile), ω is the laser frequency, τ is the time delay between the two pulses, and ϕ_i ($i = 1$ and 2) are the optical phases of the pulses. The equation of motion of the system, the Liouville equation, that governs the time evolution of the system is[49]

$$\frac{\partial \boldsymbol{\rho}}{\partial t} = \frac{1}{i\hbar}[H_0 + H_{\text{int}}, \boldsymbol{\rho}] + \left(\frac{\partial \boldsymbol{\rho}}{\partial t}\right)_{\text{relaxation}} \quad (2)$$

where $\boldsymbol{\rho}$ is the density matrix, H_0 is the Hamiltonian of the system at the equilibrium state, H_{int} is the interaction of the external electric field with the system, and $(\partial\boldsymbol{\rho}/\partial t)_{\text{relaxation}}$ represents various relaxation processes. For a three-level system, the Liouville equation can be expressed as nine coupled differential equations of the corresponding density matrix elements that include three population and six polarization terms:

$$\frac{\partial \rho_{00}}{\partial t} = -\frac{i}{\hbar}(V_{01}\rho_{10} + V_{02}\rho_{20} - \rho_{01}V_{10} - \rho_{02}V_{20}) + \frac{\rho_{11}}{T_1^{10}} + \frac{\rho_{22}}{T_1^{20}} \quad (3)$$

$$\frac{\partial \rho_{11}}{\partial t} = -\frac{i}{\hbar}(V_{10}\rho_{01} + V_{12}\rho_{21} - \rho_{10}V_{01} - \rho_{12}V_{21}) + \frac{\rho_{22}}{T_1^{21}} + \frac{\rho_{11}}{T_1^{10}} \quad (4)$$

$$\frac{\partial \rho_{22}}{\partial t} = -\frac{i}{\hbar}(V_{20}\rho_{02} + V_{12}\rho_{12} - \rho_{20}V_{02} - \rho_{21}V_{12}) - \frac{\rho_{22}}{T_1^{20}} - \frac{\rho_{22}}{T_1^{21}} \quad (5)$$

$$\frac{\partial \rho_{01}}{\partial t} = -\frac{i}{\hbar}[\rho_{01}(E_0 - E_1)] - \frac{i}{\hbar}(V_{01}\rho_{11} - \rho_{00}V_{01} + V_{02}\rho_{21} - \rho_{02}V_{21}) - \frac{\rho_{01}}{T_2^{10}} \quad (6)$$

$$\frac{\partial \rho_{02}}{\partial t} = -\frac{i}{\hbar}[\rho_{02}(E_0 - E_1)] - \frac{i}{\hbar}(V_{01}\rho_{12} + V_{02}\rho_{22} - \rho_{00}V_{02} - \rho_{01}V_{12}) - \frac{\rho_{02}}{T_2^{20}} \quad (7)$$

$$\frac{\partial \rho_{12}}{\partial t} = -\frac{i}{\hbar}[\rho_{12}(E_1 - E_2)] - \frac{i}{\hbar}(V_{10}\rho_{02} + \rho_{12}V_{22} - \rho_{10}V_{02} - \rho_{11}V_{12}) - \frac{\rho_{12}}{T_2^{21}} \quad (8)$$

plus the complex conjugates of eqs 6−8, where $\rho_{10} = \rho_{01}^*$, ρ_{20}

$= \rho_{02}^*$, $\rho_{21} = \rho_{12}^*$, and ρ_{ij} (i and $j = 0-2$) are the density matrix elements of a three-level system, E_i is the energy of level i, and $V_{ij} = \langle i|H_{\text{int}}|j\rangle$ is the matrix element of the interaction. With the semiclassical and dipole interaction approximations, the interaction can then be expressed as $V_{ij} = -E\langle i|\boldsymbol{\mu}|j\rangle = -E\cdot\mu_{ij}$, where μ_{ij} is the transition dipole moment. Note that the population and polarization relaxation of the system are described as population decay and dephasing rates, $1/T_1^{ij}$ and $1/T_2^{ij}$ (i and $j = 0-2$) as discussed before. The frequently applied rotating wave approximation is not used here, thereby preserving contributions of the double-frequency component oscillation to the interferogram.[54]

The nine coupled differential equations describing the dynamics of a three-level system were solved numerically (Fortran program) to obtain the time evolution of the population and the polarization associated with the three-level system. The transition dipoles between neighboring states are all set to be equal and are assumed to be 10 times greater than the nonlinear transition dipole terms (i.e., $\mu_{01} = \mu_{12} = 10\mu_{02}$) in the calculation. The total polarization, $P = \text{Tr}[\boldsymbol{\rho}\cdot\boldsymbol{\mu}]$, was evaluated as a function of the delay time by integration over the data-acquisition time, which is considered to be infinitely long compared with the two-pulse delay time scale. The observable SHG signal measured with a square-law detector is thus

$$I_{\text{SHG}}(\tau) = |P_{\text{SHG}}(\tau)|^2 \propto |\int \rho_{20}\, \mathrm{d}t|^2 \qquad (9)$$

where P_{SHG} is the 2ω component of the material polarization with negligible contributions from terms besides ρ_{20}.

III. Experimental Section

A. Samples. The Ag colloids were prepared according to published methods.[55] Briefly, an aqueous solution containing silver cations was reduced to colloidal Ag^0 in the presence of citrate that acts as a stabilizer. The solution immediately turned yellow, indicating the formation of colloidal Ag particles. The average particle diameter has been determined to be 75 nm by transmission electron microscopy and atomic force microscopy. The sample was made by spin-coating the solutions onto glass coverslips. The concentration of the solution was diluted to minimize aggregation upon spin-coating. The low particle density on the substrate also ensured that individual particles could be resolved by far-field optical microscopy.

B. Apparatus. The experimental setup, shown in Figure 1, consists of three parts: a femtosecond laser system, a Mach−Zender interferometer, and an inverted optical microscope integrated with an atomic force microscope (AFM; Digital Instruments, Bioscope).

A detailed description of the laser system has been given elsewhere.[53] Briefly, femtosecond laser pulses were generated by a home-built cavity-dumped Ti:sapphire (CDTS) oscillator. Cavity dumping was achieved by an acousto-optic modulator in the laser cavity. The CDTS oscillator produced 35 nJ pulses at repetition rates from 10 to 500 kHz. The pulse energy and the average power delivered to the samples were independently adjusted by the radio frequency power and the repetition rate of a Bragg cell driver, respectively. A pair of Brewster cut BK7 prisms were used to precompensate the dispersion resulting from propagation through the material of the optics located in the light path. The pulse width was characterized by second-order interferometric autocorrelation measurements. Pulse durations as short as 23 fs, assuming a Gaussian intensity profile, were obtained at the focus of a high numerical-aperture oil-immersion objective. The laser spectrum was centered at 800 nm with a full width at half-maximum (fwhm) bandwidth of 43 nm.

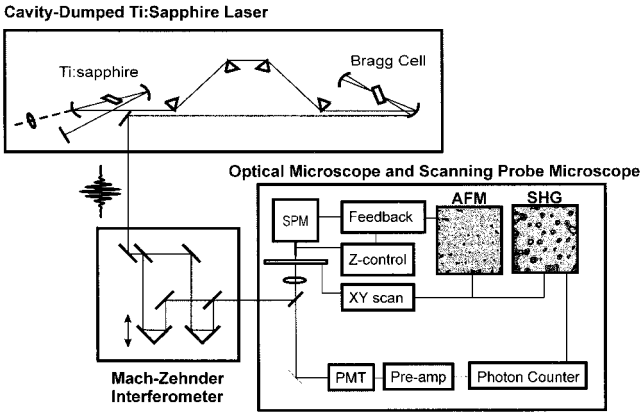

Figure 1. Experimental setup for the investigations of single colloidal Ag particles consisting of a CDTS oscillator, a Mach−Zender interferometer, an optical microscope, and a scanning probe microscope. For clarity, the prism compressor, the telescope, the phase-compensating setup, and the diagnostic reference beams are not shown. See text for details.

The pulses from the CDTS oscillator were split, delayed, and recombined collinearly in the interferometer. The delay between the pulse pair was varied by a piezo-actuated stage. The typical scan range and step size were 200 and 0.1 fs, respectively. The nonlinearity of the piezo actuator was calibrated over the whole piezo scan range, with interferometric fringes generated by a continuous wave (CW) laser (Melles-Griot, red He−Ne, $\lambda =$ 632.8 nm). Data were only taken in one scan direction to remove the error due to piezo hysteresis.

The two "exit ports" of a Mach−Zender interferometer were used in the experiment. The laser pulse-pair train exiting from one "port" of the interferometer was sent to the optical microscope and focused by an objective to the surface of a nonlinear crystal placed on a coverslip glass (the same types of coverslips were also used for sample substrates). Index-matching oil was used to provide optical contact between the cover glass and the doubling crystal. The other pulse-pair train from the second exit port (termed "reference") was focused by an achromatic lens to another nonlinear crystal for the simultaneous measurement of the reference laser pulse interferogram. The prism compressor was adjusted such that near-transformed-limited pulses were obtained at the focus of the objective. Because the dispersion of the objective is greater than that of the lens, additional material (fused silica) was added to the reference optical path until the pulse autocorrelation obtained at the reference path was virtually identical to that obtained at the focus of the objective. The doubling crystal at the focus of the objective was then replaced by the sample.

Because of the low photon count rate in the single-particle experiment, several scans need to be acquired and averaged to obtain interferograms of sufficient signal-to-noise ratio to determine the dephasing time. Signal-averaging interferometric experiments usually require active stabilization and closed-loop feedback to control the time-delay shift and phase drift that inevitably washes out the fringe contrast and can produce an artificially broadened interferogram.[56] In the present case, we use a simple approach to deal with the aforementioned errors by "aligning" the interferograms with a numerical calibration of the phase shift.

A He−Ne laser was injected into the interferometer in a counter-propagating direction with respect to the femtosecond

pulse train to generate a CW interferogram. The CW interferogram was then used to obtain the "phase" drift (actually probably time drift) of individual scans by comparing it with an ideal sinusoidal function of the 15 802.8 cm^{-1} laser frequency; the choice of the phase was arbitrary and was selected to be in-phase with the first interferogram measured. The numerically determined overall phase/time shift for each interferogram was then compensated before signal averaging. Further, the interferometer was set up in an acoustic isolation enclosure to reduce incidental phase fluctuations due to air flow and acoustic noise. Compared with the "phase-locking" technique[51,57] that requires a spectrometer and a lock-in amplifier to continuously monitor the phase/time drift at each fringe and a second piezo to actively compensate the drift, the present approach is easier to implement, relying on negligible phase/time drift over the 10 s duration of each scan. Because no significant degradation in the peak-to-wing ratio of the resultant interferogram (either pulsed or CW) averaged over 100 repetitive scans was found, the drift of the interferometer has been properly corrected, and the interferometer is "passively" stable over the duration of each individual scan.

The pulse train from the interferometer was directed into an inverted optical microscope (Carl Zeiss, Axiovert 100) and was focused to the sample by a high numerical-aperture microscope objective (Carl Zeiss, F-Fluar 40X/1.30 oil). The 700 nm diameter focal spot size (i.e., point-spread function) was obtained by laterally scanning a sharp razor blade across the focal plane.[53] The two-photon point-spread function is considerably smaller. The SHG signal generated from the sample or a KDP doubling crystal, the latter used for in situ pulse autocorrelation measurements, was collected by the same objective and directed to a thermoelectrically cooled photomultiplier tube (Hamamatsu, R4220P) for photon-counting detection. A broad-band interference filter centered at 400 nm (Melles−Griot, 03-FIB-002) and a heat-reflecting mirror (Corion, HR-750-F) were used to isolate the SHG signal from the scattered fundamental.

The pulse energy and the repetition rate need to be carefully adjusted to avoid photoinduced damage or thermal effects due to excessive laser illumination. A typical repetition rate is 250 kHz or less. The pulse energy at the focal plane is about 25 pJ, assuming 80% transmission for the objective at 800 nm, giving an energy density of 5.1 $\mu J/cm^2$. Under these conditions, the signal level remained constant, and no degradation of the interferogram was found over many hours, indicating that no photoinduced or thermal damage occurred to the single particle.

A capacitance-feedback-controlled XY stage (Queensgate Instrument, S3000) is used for sample positioning and scanning. An AFM (Digital Instruments, Bioscope) is mounted on top of the sample stage of the inverted microscope for surface characterization. This arrangement allows the same area of the surface to be accessible to the optical excitation/detection as well as to the AFM for correlated structure−function studies of heterogeneous systems. The particles are optically identified with two-photon microscopy,[58,59] where the sample is scanned with respect to the laser focal spot and the SHG signals are recorded in a point-by-point fashion to generate optical images. The SP-enhanced SHG signals from the Ag colloids are significantly greater than the SHG signals from the glass−air interface. A confocal aperture before the detector further reduces the unwanted background signals. The contrast in the optical images facilitates the definite identification of single Ag colloids. Furthermore, atomic force microscopy topographic imaging with the tip prealigned to the optical axis of the microscope (i.e., the objective field of view) was used to verify that only one particle at a time was under laser illumination. The single particle is then positioned to the center of the laser focal spot for interferometric measurement.

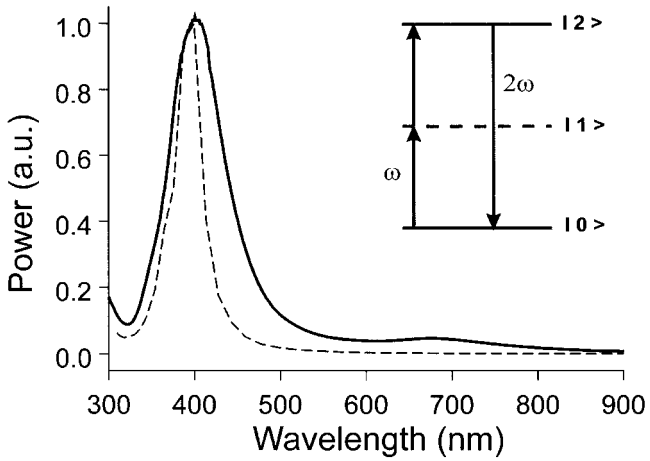

Figure 2. Linear absorption spectrum of a Ag colloidal solution (solid line) and calculated spectrum (dashed line) based on Mie theory and the dielectric constants of bulk Ag. Inset: schematic of the three-level system relevant to the density matrix calculation.

IV. Results

Linear Absorption Spectra. The linear absorption spectrum of the Ag colloidal solution is shown in Figure 2. The main resonance feature, centered at 400 nm, is associated with the collective electron−plasma oscillation.[2] Note that the "absorbance" in the spectral range of the laser fundamental (800 nm) is likely the result of Mie scattering from high aspect ratio particles.[6,60,61]

The Mie expression for the absorption cross section of spherical particles embedded in a dielectric medium is[2]

$$\sigma(\lambda) = \left(\frac{18\pi NV n_m^3}{\lambda}\right)\frac{\epsilon_2(\lambda)}{[\epsilon_1(\lambda) + 2n_m^2]^2 + \epsilon_2(\lambda)^2} \qquad (11)$$

where N is the number density of particles, V is the particle volume, n_m is the refractive index of the medium, λ is the wavelength, and $\epsilon_1(\lambda)$ and $\epsilon_2(\lambda)$ are the real and imaginary dielectric constants of the particles, respectively. This expression predicts a Lorentzian line profile with the resonance position determined by $\epsilon_1(\lambda) = -2n_m^2$. The width of the Lorentzian is determined by the imaginary part of the dielectric constant, $\epsilon_2(\lambda)$, that is directly related to the damping of the plasma oscillation. Because the dielectric constants of small particles are not well-known, the value of bulk Ag was assumed. The wavelength-dependent dielectric constants of bulk silver were taken from the literature.[62] The refractive index of the medium, i.e., water, used in the calculation is 1.332.[63] The calculated spectrum based on Mie theory is shown in Figure 2 (dashed line) overlaid on the measured spectrum. Both spectra are normalized to the peak of the plasma absorption band to clearly show the difference in the line width and profile.

Simulation. The SHG intensity, $|\int \rho_{20}\, dt|^2$, is calculated, as described in the Theory and Background section, as a function of the two-pulse delay time, τ, for different dephasing times. The results for two representative cases, $T_2^{20} = 1$ and 20 fs, are shown in Figure 3; the calculation uses a 23 fs fwhm Gaussian pulse centered at 800 nm (12 500 cm^{-1}). For dephasing times much shorter than the pulse width (e.g., $T_2^{20} = 1$ fs), the simulated autocorrelation is essentially identical with the second-

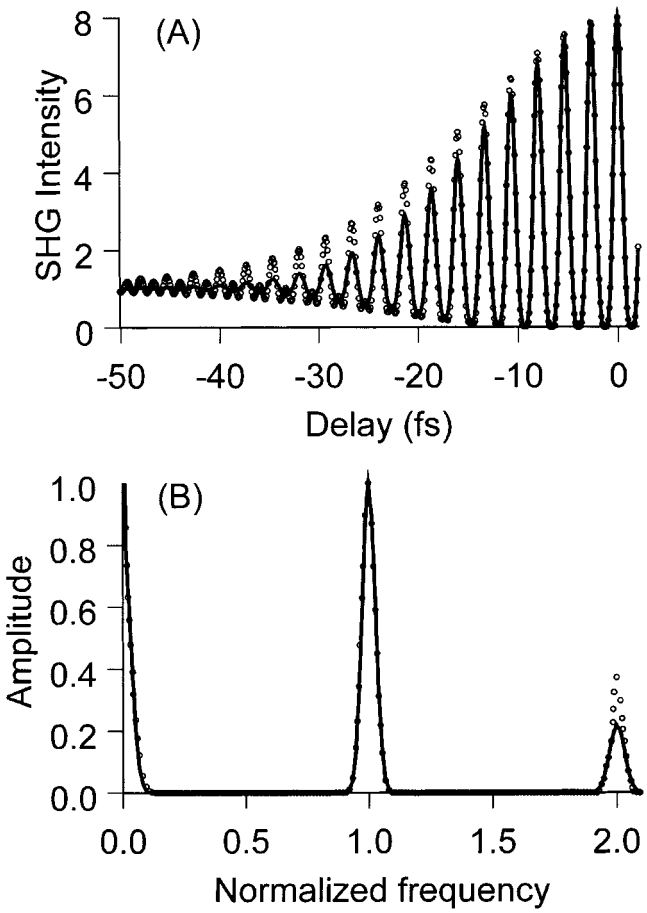

Figure 3. (A) Comparison of the simulated second-order interferometric autocorrelation functions assuming dephasing times of 1 (dark line) and 20 fs (open circles), respectively. For clarity, only one side of the symmetric autocorrelation is shown. (B) Fourier transform spectra of the autocorrelation functions.

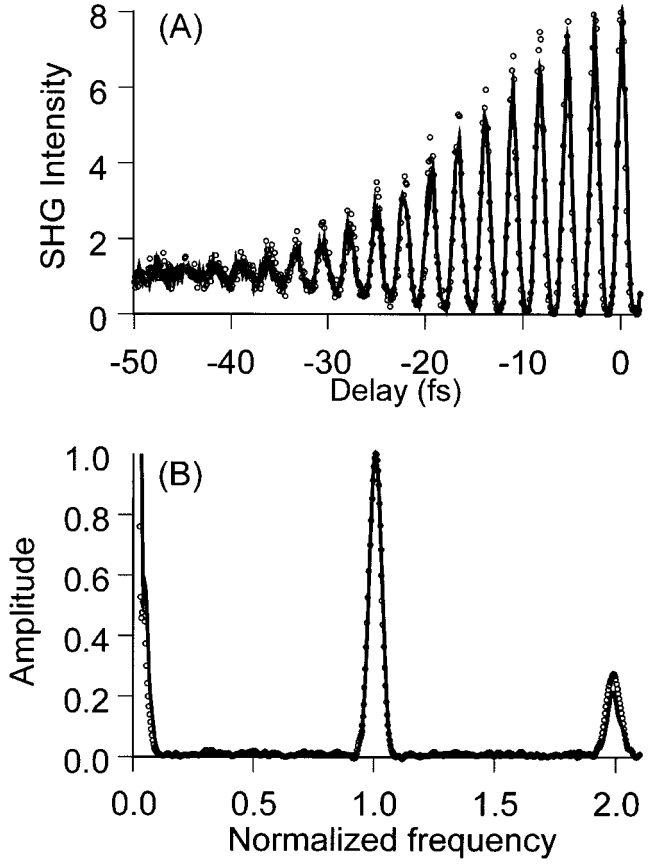

Figure 4. (A) Interferometric autocorrelation of SPs in single Ag colloidal particles (open circles) overlaid with SHG autocorrelation of laser pulses (dark line) measured from KDP crystal at the focus of the same objective. (B) Fourier transform spectra of the measured autocorrelation functions.

order pulse autocorrelation measured with a nonresonant doubling crystal (termed the reference measurement). By contrast, the autocorrelation is broadened and new frequency components appear if the dephasing time of the system is comparable with the pulse duration (e.g., $T_2^{20} = 20$ fs). Note the frequency-doubled features in Figure 3A (open circle results) that are prominent at larger delay times.

The comparison can also be made in the frequency domain. The Fourier transforms of the simulated autocorrelations are shown as the power spectra in Figure 3B normalized to the fundamental-frequency component (i.e., at ω). The double-frequency component (i.e., 2ω) in the power spectrum of the 20 fs dephasing-time simulation is significantly greater than that for the 1 fs dephasing time. The difference becomes greater as the dephasing time is further increased. As a result, the double-frequency component is used as a fingerprint of the noninstantaneous response or dephasing time of the system. An empirical relation between the dephasing time and the value of the double-frequency components in the power spectrum can thus be established from a series of simulations corresponding to different dephasing times. The result will be used to extract the dephasing time of the single Ag colloid from the experimental data.

Interferometric Autocorrelation. The SHG interferogram measured from a doubling crystal is used to characterize the pulse duration at the focus of the objective. The high numerical-aperture objective used in the present study, with a small depth of field, causes the SHG to be generated in the small focal volume ($\sim 1\ \mu m^3$), where the power density is highest. The confocal aperture further blocks signals outside the focal volume. Because the focus was set to be at the front surface (the surface close to objective) of the doubling crystal, the signal measured is mostly generated within the confocal length of the oil−crystal interface.

The SHG interferogram for single Ag colloidal particles is measured simultaneously with and in the same manner as that used to characterize the pulse duration. Both outputs of the interferometer are used to simultaneously record a reference and signal interferogram. Figure 4A shows the SHG autocorrelation of a single Ag colloid as an average over 80 consecutive scans. The laser pulse autocorrelation measured from a nonresonant KDP crystal (i.e., simultaneously acquired "reference") is overlaid for comparison. The SHG autocorrelation of a single Ag colloid is significantly broader than the measured pulse second-order autocorrelation. The power spectra of the Ag SHG interferogram and pulse autocorrelation are shown in Figure 4B. The finite dephasing time of the single Ag colloid autocorrelation manifests itself as a larger amplitude of the double-frequency component.

The noise statistics for single-photon counting are given by the Poisson distribution function with a variance equal to the averaged counts acquired per data point (i.e., per time delay channel) and thus could introduce artificial broadening. To determine the significance of noise-induced broadening of the signal, the autocorrelation of 23 fs Gaussian pulses with a per channel signal level that was assumed Poisson-distributed was calculated. The SHG autocorrelation was calculated assuming a "signal counting rate" of 150 counts/s when the sample is

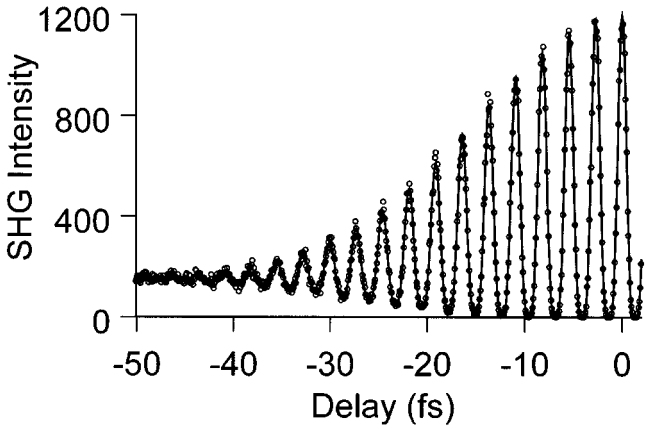

Figure 5. Simulated interferometric autocorrelation assuming a Poisson distribution in the fluctuation of the photon counts (open circles). The solid line shows the ideal interferogram with no noise. A pulse width of 23 fs and an averaged counting rate of 150 count/s are assumed in the calculation.

illuminated by two temporally nonoverlapped laser beams (i.e., the delay time ≫ the pulse width). A Poisson distribution function was generated for each data point, with the average of the distribution being the value of the data point. The noisy autocorrelation was then calculated by sampling the data from the associated Poisson distribution. The result of the calculations is shown in Figure 5. The almost imperceptible broadening resulting from noise clearly is not the origin of the temporal broadening shown in Figure 4. As a result, the measured broadening can be attributed to the coherent interaction of photons with, and the finite dephasing time of, the Ag colloidal particle SP.

The dephasing time was determined to be 10 fs by comparing the measured interferogram to the results of simulations for different dephasing times. Figure 6 shows the calculated autocorrelation function corresponding to a 10 fs dephasing time overlaid with the experimental result of the single Ag colloid. The measurement is reproduced well by the simulation.

V. Discussion

The calculated spectrum of silver particles based on Mie theory shown in Figure 2 is in good agreement with the measured peak position, indicating that the real part of the dielectric constant of silver particles does not differ significantly from that of the bulk material. The discrepancy in the spectral width is obvious. The fwhm of the calculated spectrum is 0.25 eV (2000 cm^{-1}), corresponding to a dephasing time of 5.3 fs. By comparison, the 0.6 eV fwhm of the measured spectrum would give a dephasing time of 2.2 fs, assuming the spectral width is homogeneously broadened (from the damping of the SP). Although the spectral width is a manifestation of the dynamics, the complex nature of the spectral width makes this simple estimation questionable.

We suggest that the broad spectral width of the colloidal solution results mainly from the inhomogeneity of the system; it is static in nature, resulting from the polydispersity of the particle size and shape. Because a sample can never be prepared with identical particles, this effect will always be present. Also, variations in the local environment of each particle cause the resonance of individual particles to be different from one another, causing the measured static spectrum to be broader than the spectrum of each single particle. Fluctuations in the local environment caused by solvent motion might also cause the peak position to fluctuate (causing the width to increase) because of changes in the dielectric constant of the medium.[50]

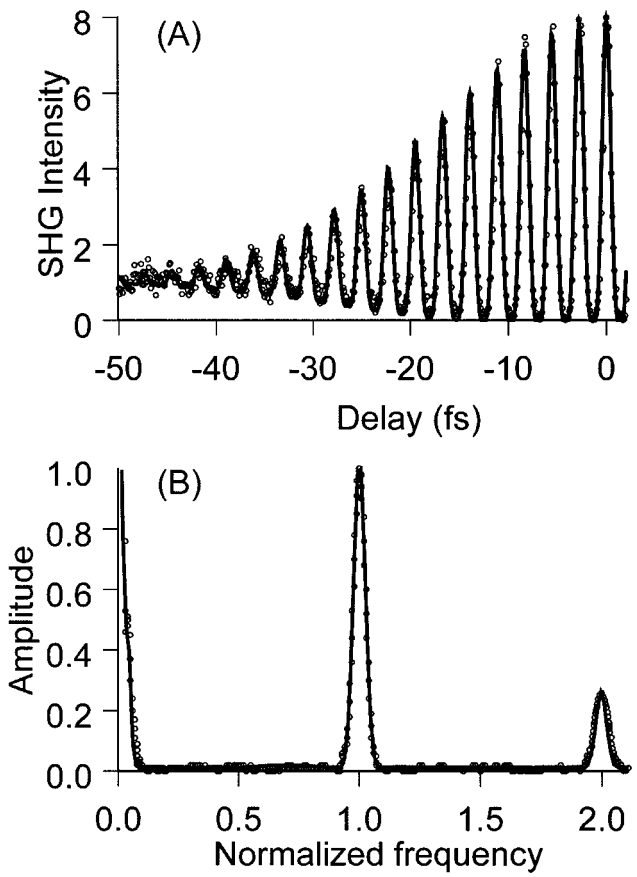

Figure 6. (A) Interferometric autocorrelation of SPs in single Ag colloidal particles (open circles) overlaid with the simulation (dark line) assuming a 10 fs dephasing time (i.e, $T_2^{20} = 10$ fs). (B) Fourier transform spectra of the autocorrelation functions.

Nonlinear (e.g., photon-echo) spectroscopy is one method used to separate the inhomogeneous and homogeneous contributions to dephasing dynamics. However, the extremely rapid dephasing time implied by the line width and the 10 fs T_2 measured here makes this measurement very challenging. In principle, it is possible to measure the absorption spectrum on single nanoparticles; the actual measurement, however, is usually hindered by low optical density. The free-induction decay acquired by a two-pulse first-order (electric-field) interferogram measured on single particles provides the same information, but it also encounters a similar optical density/sensitivity problem. A higher order spectroscopic measurement of single chromophores provides an opportunity to circumvent this difficulty. SHG of the Ag colloids dominates any background signal because of the plasmon resonance enhancement. As a result, the free-induction decay of single nanoparticles can be obtained by a second-order two-pulse interferometric autocorrelation measurement even with the small optical density presented by a single particle.

The observed interferometric autocorrelation of the Ag particles can be understood in the following way. The plasmon oscillation driven by the laser field will eventually lose the phase information (coherence) because of pure dephasing processes such as elastic electron−electron scattering. Other energy dissipation processes such as inelastic electron−electron scattering, radiative decay, and electron−phonon scattering will also contribute to the damping. These damping processes manifest themselves as the optical conductivity or as the imaginary part of the dielectric function.[20] The overall decay processes modulate the measured SHG autocorrelation. If the lifetime of

the plasmon oscillation is comparable to or longer than the laser pulse duration, the driven polarization will last longer than the laser field oscillation and cause the broadening of the autocorrelation measured in this experiment.

It is noteworthy to compare the present results with recent studies on the dephasing dynamics of SPs in noble metal systems. There is only one report on the dephasing time of single particles to date.[42] In this frequency−domain study, the near-field extinction spectra of individual Au particles were measured. The dephasing time extracted from the homogeneous spectra was around 8 fs for 20 nm Au particles embedded in a TiO_2 matrix. The dephasing of SPs has been studied on several metallic systems including colloidal gold in solution,[23] gold nanoparticles embedded in a medium,[24] and silver island films.[64] Among them, a plasmon decay time of 40 fs was obtained for Ag films, and upper limits of 20 and 50 fs have been reported for gold nanoparticles[24] and colloidal gold in solution,[23] respectively. In these earlier studies, the relaxation time was estimated (indirectly) from nonlinear spectroscopy experiments or measured in the time domain with relatively poor resolution. Therefore, these values should be regarded with caution.

Recently, Aussenegg and co-workers performed a decay-time measurement of the electron−plasma oscillation of Au and Ag lithographically designed particle arrays, with a particle's lateral size being about 150 nm.[13,36,37] The reported decay time is 7−10 fs for Ag nanoparticle arrays.[36] The energy decay time is approximately equal to half of the dephasing time. As a result, the dephasing time of silver particles reported in ref 36 corresponds to 14−20 fs, slightly larger than the value obtained in the present study. The size distribution for the nanoparticles appeared to be around 10%. Because of the relatively larger illumination region, the SHG signals should contain contributions from a significant number of particles presumably having slightly different sizes and shapes. This inhomogeneity would distort the SHG autocorrelation and thus affect the decay time extracted from the ensemble measurement. Recent theoretical studies of plasmon dynamics suggest that the inhomogeneity would narrow the autocorrelation, making the determination of the decay time from the ensemble autocorrelation measurement difficult.[65] The slight inconsistency in the spectral width and the determined dephasing time also implies a residual inhomogeneity. Therefore, the decay time measured by Aussenegg and co-workers can be regarded as a lower limit for Ag particles of lateral sizes of around 200 nm. The Ag particles in the present study are considerably smaller in size. Therefore, the electrons would undergo more frequent surface-mediated electron−electron scattering, resulting in faster damping of the plasma oscillation. Also, the surrounding organic layer of the colloids would provide an additional relaxation mechanism, termed chemical-interface damping.[2] Taking these factors into account, we found that the present results are reasonably consistent with those of Aussenegg and co-workers.

VI. Conclusion

In summary, we have presented the first time-resolved studies of the SP dephasing of single Ag particles. The measured dephasing time is 10 fs for single Ag colloids of 75 nm diameter. Our results are in agreement with values obtained from measurements on particle arrays. Future work on the dephasing dynamics of single nanoparticles of different sizes and shapes is underway.

We combined time-resolved interferometric spectroscopy with multiphoton microscopy to study the single nanoparticle dynamics. The work could be extended to single chromophores such as single molecules. To obtain useful data, before photobleaching, phase-locked pulse-pair techniques[57] could be used to reduce the data-acquisition time. The ultrafast interferometric responses of single chromophores, if spectrally resolved, could provide more detailed information of homogeneous dynamics of different molecular states.[66] Both extensions are being explored.

Acknowledgment. The authors thank Dr. H. Miyoshi and Prof. James Norris for supplying aqueous solutions of Ag colloidal particles. This research was supported by the W. M. Keck Foundation (991705) and the University of Chicago MRSEC (NSF-DMR-9808595). A.N.U. thanks the Deutsche Forschungsgemeinschaft (DFG) for a fellowship. N.F.S. acknowledges the Dreyfus Foundation for a fellowship.

References and Notes

(1) Shalaev, M. V.; Moskovits, M. *Nanostructured materials: clusters, composites, and thin films*; American Chemical Society: Washington, DC, 1997.
(2) Kreibig, U.; Vollmer, M. *Optical properties of metal clusters*; Springer-Verlag: New York, 1995.
(3) Alivisatos, A. P. *Science* **1996**, *277*, 933−937.
(4) Brus, L. E. *Appl. Phys. A* **1991**, *53*, 465−474.
(5) Gotschy, W.; Vonmetz, K.; Leitner, A.; Aussenegg, F. R. *Opt. Lett.* **1996**, *21*, 1099−1101.
(6) Link, S.; Mohamed, M. B.; El-Sayed, M. A. *J. Phys. Chem. B* **1999**, *103*, 3073−3077.
(7) Link, S.; El-Sayed, M. A. *J. Phys. Chem. B* **1999**, *103*, 4212−4217.
(8) Hodak, J. H.; Henglein, A.; Hartland, G. V. *J. Chem. Phys.* **1999**, *111*, 8613−8621.
(9) Jensen, T. R.; Schatz, G. C.; Van Duyne, R. P. *J. Phys. Chem. B* **1999**, *103*, 2394−2401.
(10) Lyon, L. A.; Pena, D. J.; Natan, M. J. *J. Phys. Chem. B* **1999**, *103*, 5826−5831.
(11) Halte, V.; Bigot, J. Y.; B., P.; Broyer, M.; Prevel, B.; Perez, A. *Appl. Phys. Lett.* **1999**, *75*, 3799−3801.
(12) Kreibig, U.; Genzel, U. *Surf. Sci.* **1985**, *156*, 678−700.
(13) Lamprecht, B.; Leitner, A.; Aussenegg, F. R. *Appl. Phys. B* **1997**, *64*, 269−272.
(14) Feldstein, M. J.; Keating, C. D.; Liau, Y.-H.; Natan, M. J.; Scherer, N. F. *J. Am. Chem. Soc.* **1997**, *119*, 6638−6647.
(15) Taleb, A.; Petit, C.; Pileni, M. P. *J. Phys. Chem. B* **1998**, *102*, 2214−2220.
(16) Shiang, J. J.; Heath, J. R.; Collier, C. P.; Saykally, R. J. *J. Phys. Chem. B* **1998**, *102*, 3425−3430.
(17) Wang, W.; Feldstein, M. J.; Scherer, N. F. *Chem. Phys. Lett.* **1996**, *262*, 573−582.
(18) Liau, Y.-H.; Scherer, N. F. In *Ultrafast Phenomena XII*; Murnane, M. M., Scherer, N. F., Mukamel, S., Elsaesser, T., Eds.; Springer-Verlag: Berlin, Germany, 2001; pp 410−412.
(19) Feldstein, M. J.; Scherer, N. F. *Proc. SPIE−Int. Soc. Opt. Eng.* **1998**, *3272*, 58−65.
(20) Ashcroft, N. W.; Mermin, N. D. *Solid State Physics*; Saunders College: Philadelphia, PA, 1976.
(21) Sun, C. K.; Vallee, F.; Acioli, L.; Ippen, E. P.; Fujimoto, J. G. *Phys. Rev. B* **1993**, *48*, 12365−12368.
(22) Sun, C. K.; Vallee, F.; Acioli, L.; Ippen, E. P.; Fujimoto, J. G. *Phys. Rev. B* **1994**, *50*, 15337−15348.
(23) Heilweil, E. J.; Hochstrasser, R. M. *J. Chem. Phys.* **1985**, *82*, 4762.
(24) Puech, K.; Henari, F. Z.; Blau, W. J.; Duff, D.; Schmid, G. *Chem. Phys. Lett.* **1995**, *247*, 13.
(25) Van Exter, M.; Lagendijk, A. *Phys. Rev. Lett.* **1988**, *60*, 49−52.
(26) Groeneveld, R. H. M.; Sprik, R.; Lagendijk, A. *Phys. Rev. Lett.* **1990**, *64*, 784−787.
(27) Bigot, J. Y.; Merle, J. C.; Cregut, O.; Daunois, A. *Phys. Rev. Lett.* **1995**, *75*, 4702−4705.
(28) Roberti, T. W.; Smith, B. A.; Zhang, J. Z. *J. Chem. Phys.* **1995**, *102*, 3860−3866.
(29) Ahmadi, T. S.; Logunov, S. L.; El-Sayed, M. A. *J. Phys. Chem.* **1996**, *100*, 8053−8056.
(30) Perner, M.; Bost, P.; Lemmer, U.; von Plessen, G.; Feldmann, J.; Becker, U.; Mennig, M.; Schmitt, M.; Schmidt, H. *Phys. Rev. Lett.* **1997**, *78*, 2192−2195.
(31) Shahbazyan, T. V.; Perakis, I. E.; Bigot, J. Y. *Phys. Rev. Lett.* **1998**, *81*, 3120−3123.
(32) Hodak, J. H.; Martini, I.; Hartland, G. V. *Chem. Phys. Lett.* **1998**, *284*, 135−141.

(33) Klein-Wiele, J. H.; Simon, P.; Rubahn, H. G. *Phys. Rev. Lett.* **1998**, *80*, 45−48.

(34) Ogawa, S.; Nagano, H.; Petek, H. *Phys. Rev. Lett.* **1997**, *78*, 1339−1342.

(35) Liau, Y.-H.; Feldstein, M. J.; Scherer, N. F. In *Ultrafast Phenomena XI*; Elsaesser, T., Fujimoto, J. G., Wiersma, D. A., Eds.; Springer-Verlag: Berlin, Germany, 1998; pp 156−158.

(36) Lamprecht, B.; Leitner, A.; Aussenegg, F. R. *Appl. Phys. B* **1999**, *68*, 419−423.

(37) Lamprecht, B.; Krein, J. R.; Leitner, A.; Aussenegg, F. R. *Phys. Rev. Lett.* **1999**, *83*, 4421−4424.

(38) Yu, X. Y.; Luo, Q.; Li, L.; Li, Q.; Qiu, Z. R.; Zhou, J. Y. *Appl. Phys. Lett.* **1998**, *73*, 3321−3323.

(39) Zhang, J. Z. *Acc. Chem. Res.* **1997**, *30*, 423−429.

(40) Smith, B. A.; Zhang, J. Z.; Giebel, U.; Schmid, G. *Chem. Phys. Lett.* **1997**, *270*, 139.

(41) Averitt, R. D.; Westcott, S. L.; Halas, N. J. *Phys. Rev. B* **1998**, *58*, 10203.

(42) Kalr, T.; Perner, M.; Grosse, S.; von Plessen, G.; Spirkl, W.; Feldmann, J. *Phys. Rev. Lett.* **1998**, *80*, 4249.

(43) Liau, Y.-H.; Scherer, N. F. *Appl. Phys. Lett.* **1999**, *74*, 3966−3968.

(44) Emory, S. R.; Haskins, W. E.; Nie, S. *J. Am. Chem. Soc.* **1998**, *120*, 8009−8010.

(45) Kneipp, K.; Wang, Y.; Kneipp, H.; Perelman, L. T.; Itzkan, I. *Phys. Rev. Lett.* **1997**, *78*, 1667−1670.

(46) Xu, H.; Bjerneld, E. J.; Kall, M.; Borjesson, L. *Phys. Rev. Lett.* **1999**, *83*, 4357−4360.

(47) Krug, J. T.; Wang, G. D.; Emory, S. R.; Nie, S. *J. Am. Chem. Soc.* **1999**, *121*, 9208−9214.

(48) Michaels, A. M.; Nirmal, M.; Brus, L. E. *J. Am. Chem. Soc.* **1999**, *121*, 9932−9939.

(49) Sargent, M., III; Scully, M. O.; Lamb, J. *Laser physics*; Addison-Wesley: Reading, MA, 1974.

(50) Mukamel, S. *Principles of Nonlinear Optical Spectroscopy*; Oxford: New York, 1995.

(51) Petek, H.; Ogawa, S. *Prog. Surf. Sci.* **1997**, *56*, 239−310.

(52) Baltuska, A.; Pshenichnikov, M. A.; Wiersma, D. A. *Opt. Lett.* **1998**, *23*, 1474−1476.

(53) Liau, Y.-H.; Unterreiner, A. N.; Arnett, D.; Scherer, N. F. *Appl. Opt.* **1999**, *38*, 7386−7392.

(54) Allen, L.; Eberly, J. H. *Optical Resonance and Two-level l Atoms*; Dover: New York, 1987.

(55) Kapoor, S. *Langmuir* **1998**, *14*, 1021−1025.

(56) The issue of distinguishing time-delay shift and phase shift has been addressed by Jonas and co-workers (*J. Chem. Phys. 111*, 10934). Experimentally, changes of the optical path length in the interferometer resulting from the piezo not going back to the same position for each scan will shift time-zero of the interferogram, but the shape of the individual interferograms should be identical if the laser pulse relative phase and dispersion remain constant. If an abrupt piezo drift occurs during a scan, the interferogram will not only shift in time-zero but also change shape resulting in asymmetric interferograms. An unbalanced interferometer will also result in asymmetric interferograms.

(57) Scherer, N. F.; Carlson, R. J.; Matro, Z.; Du, M.; Ruggiero, A. J.; Romero-Rochin, V.; Cina, J. A.; Fleming, G. R.; Rice, S. A. *J. Chem. Phys.* **1991**, *95*, 1487−1511.

(58) Denk, W.; Strickler, J. H.; Webb, W. W. *Science* **1990**, *248*, *73*−*76*.

(59) Blanton, S. A.; Dehestani, A.; Lin, P. C.; Guyot-Sionnest, P. *Chem. Phys. Lett.* **1994**, *229*, 317−322.

(60) Yu, Y. Y.; Chang, S. S.; Lee, C. L.; Wang, C. R. C. *J. Phys. Chem. B* **1997**, *101*, 6661−6664.

(61) Mohamed, M. B.; Volkov, V.; Link, S.; El-Sayed, M. A. *Chem. Phys. Lett.* **2000**, *317*, 517−523.

(62) Palik, E. D. *Handbook of optical constants of solids*; Academic Press: San Diego, CA, 1985.

(63) Weast, R. C. *Handbook of Chemistry and Physics*, 49th ed.; CRC: Cleveland.

(64) Steinmüller-Nethl, D.; Höpfel, R. A.; Gornik, E.; Leitner, A. A. F. R. *Phys. Rev. Lett.* **1992**, *68*, 389.

(65) Vartanyan, T.; Simon, M.; Träger, F. *Appl. Phys. B* **1999**, *68*, 425.

(66) Gruetzmacher, J. A.; Scherer, N. F. In *Ultrafast Phenomena XII*; Murnane, M. M., Scherer, N. F., Mukamel, S., Elsaesser, T., Eds.; Springer-Verlag: Berlin, Germany, 2001; pp 530−532.